

## Facile Synthesis of Composite Electrodes Containing Platinum Particles Distributed in Nanowires of Polyaniline-Poly(Acrylic Acid) for Methanol Oxidation

Chung-Wen Kuo<sup>1,\*</sup>, Chang-Cian Yang<sup>1</sup>, and Tzi-Yi Wu<sup>2,3,\*</sup>

<sup>1</sup> Department of Chemical and Materials Engineering, National Kaohsiung University of Applied Sciences, Kaohsiung 80778, Taiwan

<sup>2</sup> Department of Chemistry, National Cheng Kung University, Tainan 70101, Taiwan

<sup>3</sup> Department of Materials Engineering, Kun Shan University, Tainan 71003, Taiwan

\*E-mail: [welly@cc.kuas.edu.tw](mailto:welly@cc.kuas.edu.tw), [t0718z@hotmail.com](mailto:t0718z@hotmail.com)

Received: 14 June 2011 / Accepted: 7 July 2011 / Published: 1 August 2011

---

This work demonstrates a novel and simple route for preparing a composite that comprises platinum (Pt) nanoparticles and polyaniline (PANI) doped with poly(acrylic acid) (PAA) and hydrochloric acid (HCl) via “simultaneous doping- deposition” to obtain PANI-(PAA+HCl)-Pt composite electrodes. PANI-(PAA+HCl) is characterized using X-ray photoelectron spectroscopy (XPS) and scanning electron microscopy (SEM). XPS results indicate that PANI-(PAA+HCl) has more positively charged nitrogen atoms compared to PANI doped with HCl (PANI-HCl). SEM images reveal that PANI-(PAA+HCl) is composed of highly porous nanowires. The morphology and structure of the PANI-(PAA+HCl)-Pt composite are further characterized by transmission electron microscopy (TEM) and Auger electron spectroscopy (AES). TEM images and AES results indicate that Pt particles are dispersed uniformly into the spatial regions of PANI-(PAA+HCl). Cyclic voltammetry results and chronoamperometric response measurements show that PANI-(PAA+HCl)-Pt electrodes have good electrocatalytic activity of methanol oxidation with low CO poisoning.

---

**Keywords:** Polyaniline, poly(acrylic acid), nanowires, cyclic voltammetry, TEM, methanol oxidation

### 1. INTRODUCTION

Direct methanol fuel cells (DMFC) are highly attractive power sources for a variety of applications due to their high energy efficiency, low emissions, low noise, and environmental friendliness [1-8]. DMFCs are based on methanol electro-oxidation at the anode. Among the numerous materials used for the anode of DMFCs, Pt has been established as a powerful electrocatalyst for the oxidation of methanol [9,10]. However, the use of Pt in the form of smooth foils for the direct electro-

oxidation of methanol has been found to be inefficient due to (i) high cost and (ii) the formation of strongly adsorbed intermediates such as CO (referred to as  $\text{CO}_{\text{ads}}$ ) as a result of the dissociative adsorption of methanol [11].

In order to mitigate  $\text{CO}_{\text{ads}}$ -like poisoning, various strategies have been developed to improve the electrocatalytic activity for methanol electro-oxidation and oxygen reduction reactions, including the addition or incorporation of a second element into Pt electrocatalysts, such as catalyst supporters [12,13]. It has been shown that the use of conducting polymers (CPs) as a catalyst supporter is a simple and useful way of reducing catalyst poisoning. CPs in their various oxidation states interconvert each other, which allows a redox cycle to form for catalytic reactions. Thus, the electrochemical deposition of metals on electrodes modified with CP films is a convenient and inexpensive route for developing anode materials. Studies on CPs as host materials for Pt nanoparticles have focused on polyaniline (PANI) [14,15], polypyrrole (PPy) [16,17], and polythiophene (PT) [18] for methanol oxidation. The advantage of using CPs over other materials is that they are permeable to electroactive species, sufficiently conductive for current flow between the solution and substrate, easily modified using various techniques, and easy to coat onto various substrates. CPs also act as electrocatalyst and current collectors.

Poly(styrenesulfonic acid) (PSS), a polymer acid, has been shown to be easily incorporated in a CP matrix as a dopant as a support for Pt particles. Huang *et al.* [19] reported that PANI-PSS acts as a matrix that leads to the uniform distribution of Pt particles. As a result, the electrocatalytic activity for methanol oxidation of PANI-PSS-Pt is much higher than that of PANI-Pt. Kuo *et al.* [20] reported that highly dispersed Pt particles became homogeneously distributed in a poly(3,4-ethylenedioxythiophene)-poly(styrene sulfonic acid) (PEDOT-PSS) matrix. However, these investigations mainly focused on the manufacture of PSS as a dopant in a CP matrix; less attention has been given to the processing of a CP modified with a polymer acid containing carboxylic acid groups for use as a supporting material in DMFCs.

In the present study, a simple simultaneous doping-deposition method is used to introduce  $-\text{CO}_2\text{H}$  groups (poly(acrylic acid), PAA) and HCl with  $\text{Pt}^{4+}$  ions into a PANI matrix. PANI doped simultaneously with PAA and HCl forms a spatial network structure, which behaves as a 3D-random matrix for the deposition of Pt particles. We believe that PANI-(PAA+HCl) may act as a stabilizer for Pt particles, preventing their aggregation. The PANI-(PAA+HCl)-Pt composite is expected to enhance electroactivity for methanol oxidation.

## 2. EXPERIMENTAL

### 2.1. Preparation of PANI-(PAA+HCl)

A mixture solution of 50 mM ANI (Merck) and 0.5 M  $\text{H}_2\text{SO}_4$  (Merck) aqueous solution was prepared. Electrochemical polymerization of the solution was carried out using a potentiostatic method with stainless steel 316 (SS) as the working electrode for a total charge of  $0.1 \text{ C cm}^{-2}$ , details of the procedure are described elsewhere [21]. Before each experiment, SS was cleaned in an ultrasonic bath

using detergent, deionized water, and isopropanol, and then dried with a dry nitrogen flow. The electrochemically deposited PANI film was rinsed with double distilled water for 5 min and then dried at 120 °C for 3 min. The Emeraldine base form (EB) of PANI was obtained by treating the PANI film in 0.1 M ammonium hydroxide (Aldrich) for 3 min. The EB film was then simultaneously redoped with poly(acrylic acid) (PAA) ( $M_w = 450,000$ , Aldrich) and HCl in 0.01 M PAA + 0.01 M HCl solution containing 5 mM  $H_2PtCl_6 \cdot 6H_2O$ . EB film redoped with PAA and HCl is denoted as PANI-(PAA+HCl). For comparison, EB film was redoped with HCl in 0.01 M HCl solution containing 5 mM  $H_2PtCl_6 \cdot 6H_2O$  (denoted as PANI-HCl).

## 2.2. Deposition of Pt into PANI-(PAA+HCl) matrix

Pt particles were incorporated into PANI-(PAA+HCl) film via electrochemical deposition from 0.01 M PAA + 0.01 M HCl + 0.1 M KCl solution containing 5 mM  $H_2PtCl_6 \cdot 6H_2O$  (PANI-(PAA+HCl)-Pt) with a constant deposition charge of 0.15 C at a constant potential of -0.2 V (vs. Ag/AgCl). For comparison, Pt particles were also deposited into a PANI-HCl matrix (PANI-HCl-Pt) under deposition conditions similar to those used for PANI-(PAA+HCl). After Pt particle incorporation, the electrodes were rinsed with double distilled water for 5 min and then dried at 120 °C for 3 min. The amount of Pt loaded into PANI-(PAA+HCl) or deposited onto PANI-HCl was calculated using:

$$m = \frac{Q_{dep} \cdot M}{F \cdot Z}$$

where  $M$  is the atomic weight of Pt,  $F$  is the Faradic constant, and  $Z$  is the number of electrons transferred (taken as four for the formation of Pt). The amount ( $m$ ) was calculated using the charge ( $Q_{dep}$ ) utilized for the deposition of Pt particles.

## 2.3. Characterization of PANI-(PAA+HCl)-Pt composite electrode

A X-ray photoelectron spectroscopy (XPS) study was performed using an ESCA 210 spectrometer with Mg K  $\alpha$  ( $h\nu = 1253.6$  eV) irradiation as the photon source. The primary tension was 12 kV and the pressure during the scans was approximately  $10^{-10}$  mbar. The surface morphologies of PANI-(PAA+HCl)-Pt and PANI-HCl-Pt films were compared using a scanning electron microscope (SEM) (JEOL JSM-6700F) equipped with an energy dispersive spectroscopy (EDS). The morphology was characterized by Transmission electron microscopy (TEM, JEOL 1200 EX) at a 100 kV accelerating voltage. Specimens for TEM were prepared by spreading a small drop of one of the sample solutions onto a 400-mesh copper grid. The drop was dried in air at room temperature for nearly 4 days. Auger electron spectroscopy (AES) depth profiles were obtained with a Microlab 310 D (VG Scientific Ltd.) spectrometer at emission currents of 0.1 and 8 mA with gun tensions of 10 (electron) and 3 kV (ion), respectively.

Electrochemical characterizations of PANI-(PAA+HCl)-Pt and PANI-HCl-Pt composite electrodes were carried out using an CHI627D electrochemical analyzer (U.S.A.). All experiments were performed in a three-component cell.

An Ag/AgCl electrode (in 3 M KCl), Pt wire, and SS (1-cm<sup>2</sup> area) were used as the reference, counter, and working electrodes, respectively. A Luggin capillary, whose tip was set at a distance of 1-2 mm from the surface of the working electrode, was used to minimize errors due to  $iR$  drop in the electrolytes.

#### 2.4. Methanol Electro-oxidation and Stability of PANI-(PAA+HCl)-Pt composite electrode

The catalytic activities of PANI-(PAA+HCl)-Pt and PANI-HCl-Pt composite electrodes were examined by cyclic voltammetry (CV) at 10 mV sec<sup>-1</sup> ranging from -0.2 to 1.0 V. Chronoamperometric response curves were obtained at 0.6 V in 0.1 M CH<sub>3</sub>OH + 0.5 M H<sub>2</sub>SO<sub>4</sub> solution. All the electrochemical experiments were carried out at room temperature.

### 3. RESULTS AND DISCUSSION

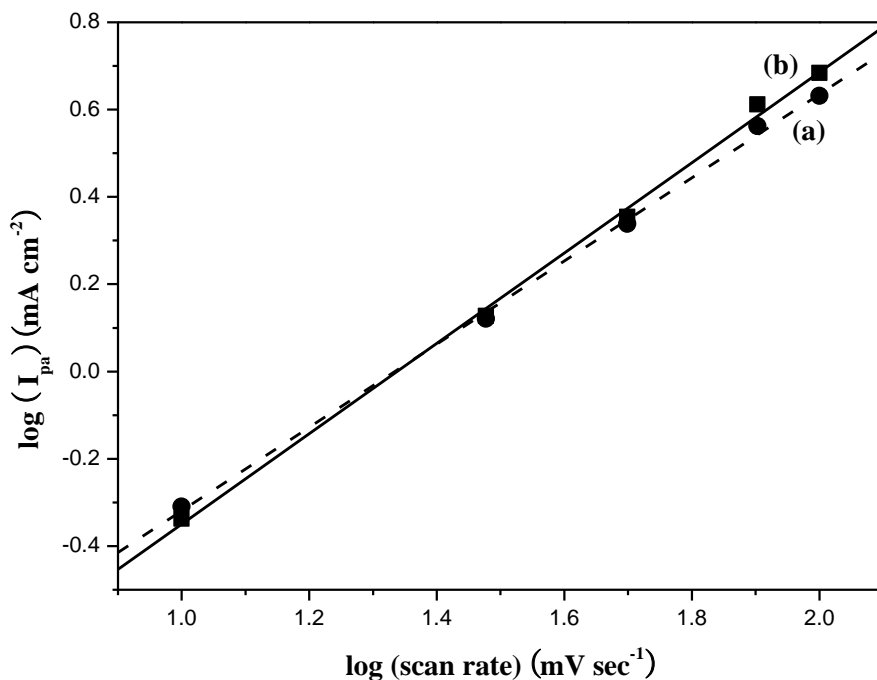
#### 3.1. Characterizations of PANI-(PAA+HCl)

An investigation was made into the charge transport mechanism in the PANI-(PAA+HCl)-Pt and PANI-HCl-Pt composite electrodes at various scan rates ( $\nu$ ) by linear sweep voltammograms (LSVs). The double logarithmic plots of peak current versus  $\nu$  (Fig. 1) for the two types of electrode are linear with nearly identical slopes.

It is known that the linearity of a plot of peak current versus  $\nu$  corresponds to the surface-bound transport process and a different type of linear for the plot of peak current versus  $\nu^{1/2}$  signifies a diffusion control process [22]. The slope values of the double logarithmic plots are 0.95 and 1.03 for PANI-HCl and PANI-(PAA+HCl), respectively. Thus, the PANI-HCl and PANI-(PAA+HCl) composite electrodes have surface-bound transport processes.

XPS analyses of the surfaces of PANI-HCl and PANI-(PAA+HCl) were conducted to investigate variations at nitrogen binding sites. Fig. 2 shows the XPS spectra of core-level N<sub>1s</sub> for PANI-HCl and PANI-(PAA+HCl).

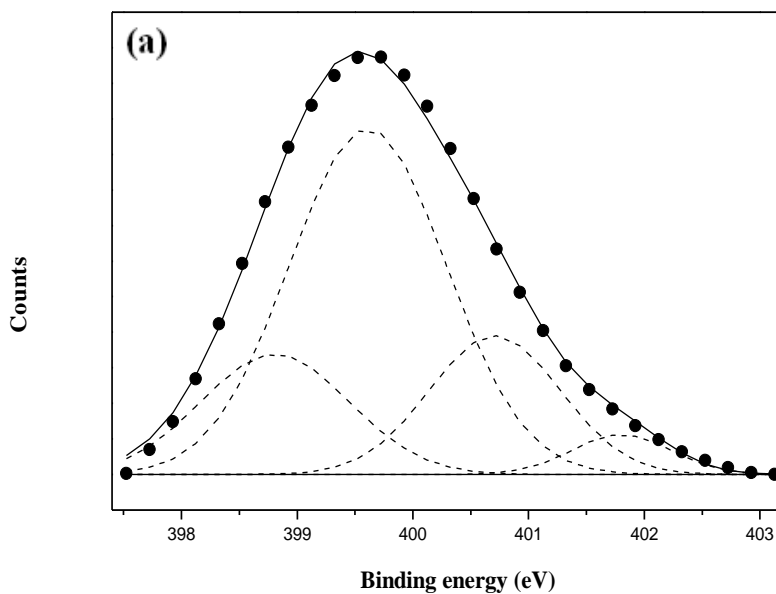
The signals of N<sub>1s</sub> were fitted with peaks at 398.8, 399.6, 400.7, and 401.8 eV, which correspond to quinonoid imine (=N-), benzenoid amine (-NH-), protonated amine (-N<sup>+</sup>), and protonated imine (=N<sup>+</sup>), respectively [23]. Kumar *et al.* [24,25] attributed the last two peaks to the presence of polarons (radical cations) and bipolarons (dications). The ratio of these two N<sub>1s</sub> components at 400.7 and 401.8 eV (positively charged nitrogen atoms) can be considered as a direct estimation of the doping level of PANI [26]. The area ratios of the four nitrogen constituents in PANI were calculated; their results are listed in Table 1. The doping level for PANI-(PAA+HCl) (27 %) is higher than that observed for PANI-HCl (23 %) due to the existence of PAA.



**Figure 1.** Dependence of the peak current on the scan rate by linear sweep voltammograms (LSVs): (a) PANI-HCl and (b) PANI-(PAA+HCl).

**Table 1.** XPS results of PANI-HCl and PANI-(PAA+HCl)

Electrode	=N- (%)	-NH- (%)	-N <sup>+</sup> (%)	=N <sup>+</sup> (%)	[-N <sup>+</sup> + =N <sup>+</sup> /N] (%)
PANI-HCl	19	58	19	4	23
PANI-(PAA+HCl)	23	50	21	6	27



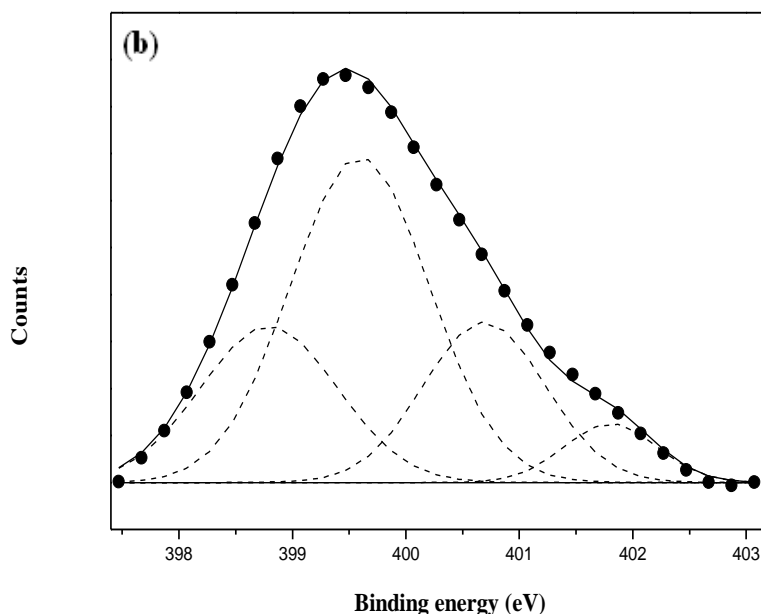
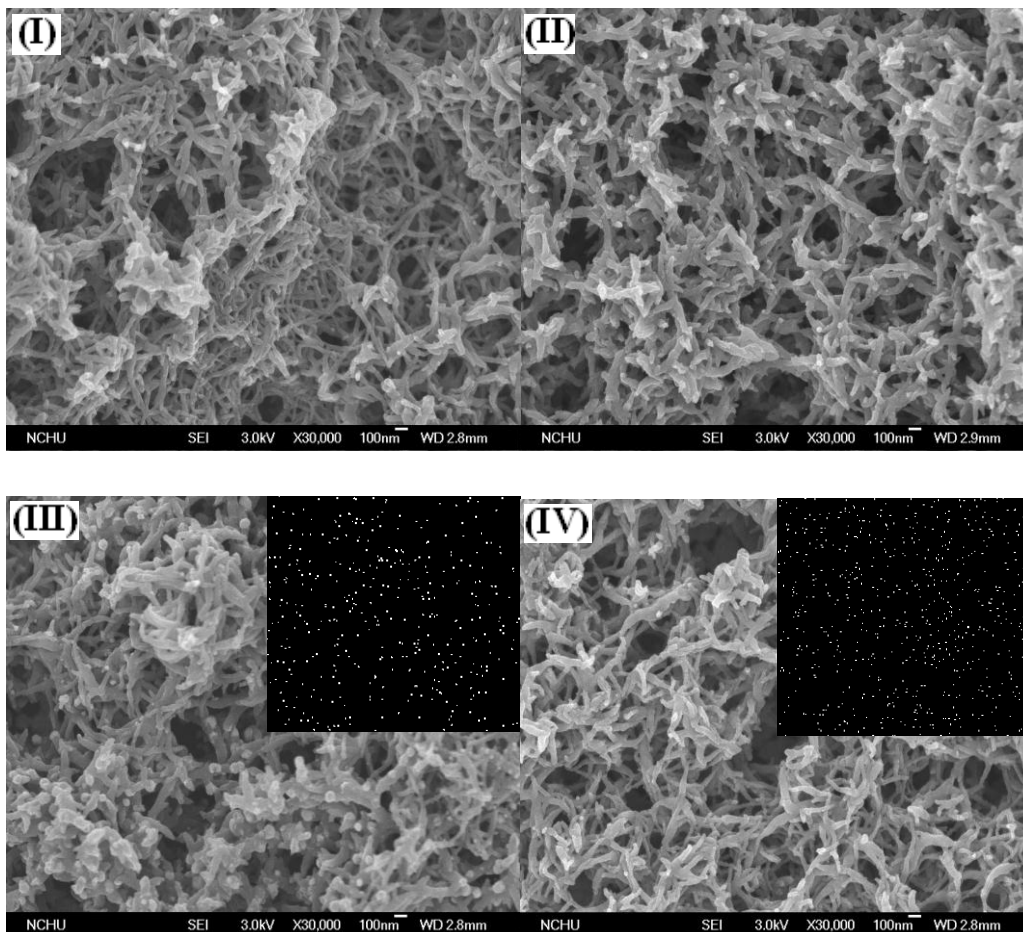


**Figure 2.**  $N_{1s}$  XPS core level spectra of (a) PANI-HCl and (b) PANI-(PAA+HCl) composite films.

### 3.2. Electrodeposition of Pt into PANI-(PAA+HCl)

Pt particles were incorporated into PANI-HCl and PANI-(PAA+HCl) films by electrochemical deposition at a constant potential of -0.2 V (vs. Ag/AgCl) with a charge of 0.15 C. Fig. 3a shows SEM micrographs of the surface morphology of PANI-HCl, PANI-(PAA+HCl), PANI-HCl-Pt, and PANI-(PAA+HCl)-Pt electrodes. The nanowire morphology for PANI-HCl and PANI-(PAA+HCl) films is clearly evident in Fig. 3a(I-II). The PANI-HCl nanowires have an average diameter of 30-60 nm. PANI-(PAA+HCl) nanowires have a larger diameter (50-80 nm) with a smooth surface due to the influence of PAA molecules on PANI. It is to be noted that the incorporation of PAA into PANI did not change the nanowire morphology. The nanowire morphology of PANI-(PAA+HCl) provides a large surface area for the subsequent deposition of Pt particles. We believe that Pt particles are incorporated into PANI-HCl and PANI-(PAA+HCl) nanowire network structures. Pt particles with a size of about 100 nm can be seen in the PANI-HCl-Pt composite electrode (Fig. 3a(III)), whereas no Pt particles are visible in the PANI-(PAA+HCl)-Pt electrode, possibly due to their small size (Fig. 3a(IV)). Even though the loading of Pt particles was low (76  $\mu\text{g}$ ), Pt particles can be clearly seen on the PANI-HCl nanowires. Pt mapping analysis for PANI-HCl-Pt and PANI-(PAA+HCl)-Pt electrodes indicates the existence of Pt (Fig. 3a inset). Fig. 3b(I-II) show a TEM micrograph of Pt particles embedded into PANI-HCl and PANI-(PAA+HCl) nanowires, respectively. The black spots indicate of Pt in PANI-HCl and PANI-(PAA+HCl). The aggregation of Pt particles can be clearly seen on PANI-HCl-Pt electrodes. The particle size of Pt (20-90 nm) for the PANI-(PAA+HCl)-Pt electrode is smaller than that for the PANI-HCl-Pt electrode, which gives the former electrode a higher active surface area. The  $\text{CO}_2^-$  groups of PAA uptake  $\text{Pt}^{4+}$  ions and HCl into the PANI matrix and PANI-(PAA+HCl) matrix, which prevents the aggregation of Pt nanoparticles after Pt formation.

(a)



(b)

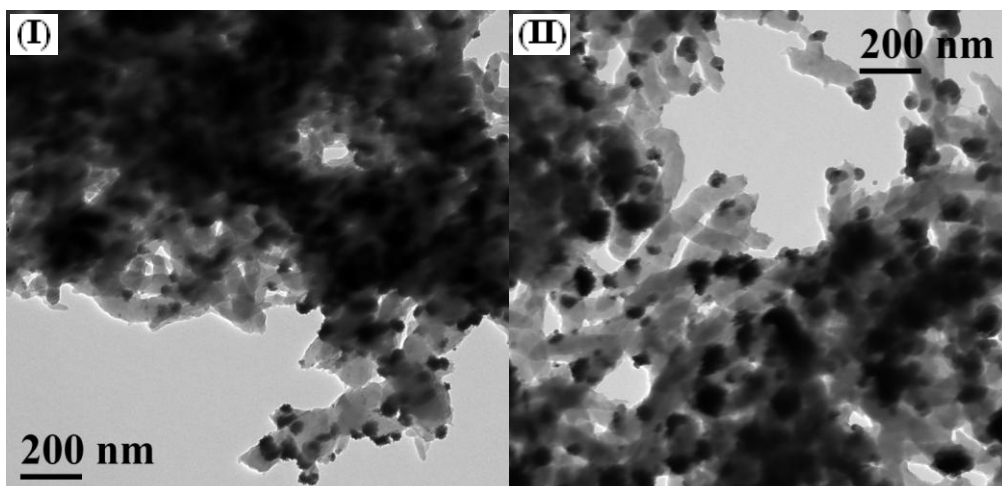


**Figure 3.** (a) SEM images of (I) PANI-HCl, (II) PANI-(PAA+HCl), (III) PANI-HCl-Pt, and (IV) PANI-(PAA+HCl)-Pt. Insets in (III) and (IV) show X-ray maps (bright spots indicate Pt). (b) TEM images of (I) PANI-HCl-Pt and (II) PANI-(PAA+HCl)-Pt.

The incorporation of Pt into PANI-HCl and PANI-(PAA+HCl) films was examined using depth profiles of Pt particles obtained with AES (Fig. 4). There is a definite difference in the

distribution of particles in PANI-HCl-Pt and PANI-(PAA+HCl)-Pt electrodes. The depth profile of Pt in the PANI-HCl matrix (curve a) increases in intensity of Pt, reaching a maximum at 2 min. The intensity then decreases rapidly after about 23 min. In contrast to the PANI-HCl-Pt electrode, Pt in the PANI-(PAA+HCl) matrix (curve b) quickly increases in intensity up to a shoulder at 2 min and then increases to a maximum at about 10 min. The intensity then decreases slowly after about 23 min. Consequently, Pt particles in the PANI-(PAA+HCl) matrix are more uniformly dispersed than those in PANI-HCl. This may be due to the  $\text{CO}_2^-$  groups of PAA uptake  $\text{Pt}^{4+}$  ions, and PANI doped with PAA and HCl form a spatial network structure that acts as a 3D-random matrix and a protective layer which prevents the aggregation of Pt particles after Pt formation. The homogenous distribution of Pt in the PANI-(PAA+HCl) spatial network structure may increase the utilization of Pt for methanol oxidation.

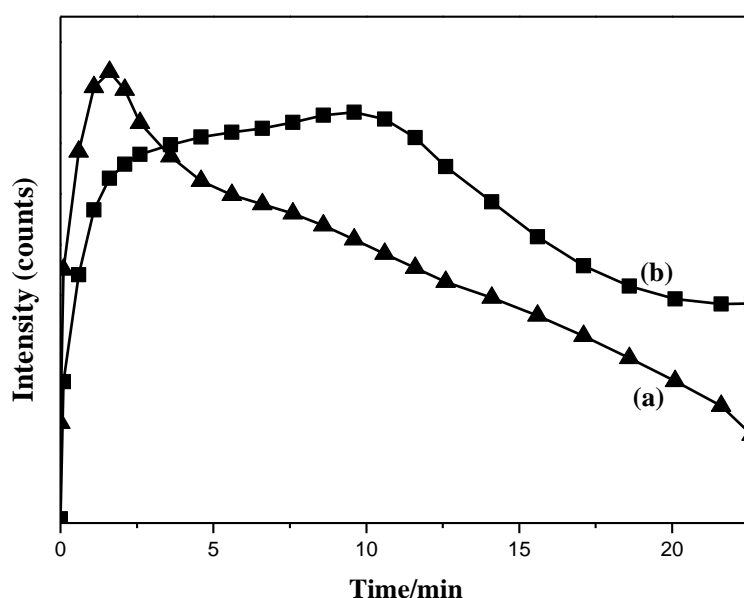


**Figure 4.** AES depth profiles for platinum within (a) PANI-HCl-Pt and (b) PANI-(PAA+HCl)-Pt.

### 3.3. Scheme of the formation of PANI-(PAA+HCl)-Pt

Based on the observed synthesis of the composite electrodes, the proposed scheme of the “simultaneous doping-deposition” of Pt in the PANI-(PAA+HCl) matrix is shown in Fig. 5. When  $\text{H}_2\text{PtCl}_6$ , HCl, and PAA are mixed well, mobile  $\text{Pt}^{4+}$  ions couple with  $\text{CO}_2^-$  groups on PAA to form a complex. During the dipping of the PANI matrix in a  $\text{H}_2\text{PtCl}_6$ , HCl, and PAA solution, PANI emeraldine base is simultaneously doped with excess  $\text{CO}_2^-$  anions on the PAA and  $\text{Cl}^-$  anions of HCl to maintain charge neutrality within the PANI phase. The formed complex ( $\text{Pt}^{4+}$  with  $\text{Cl}^-$  and  $\text{CO}_2^-$ ) may become trapped in the PANI matrix. Since Pt is deposited via a potentiostatic process, PANI-(PAA+HCl) provides an environment for the dispersion of individual Pt particles and keeps the active surface area large. We anticipate that this morphology is suitable for DMFC applications. Pt particles dispersed on a carbon black support that are used as a catalyst in DMFCs do not provide optimal

interparticle spacing for rapid methanol diffusion below the top surface layers, limiting the effectiveness of expensive catalysts. Pt particles dispersed in PANI-(PAA+HCl) may be better suited for DMFC applications.

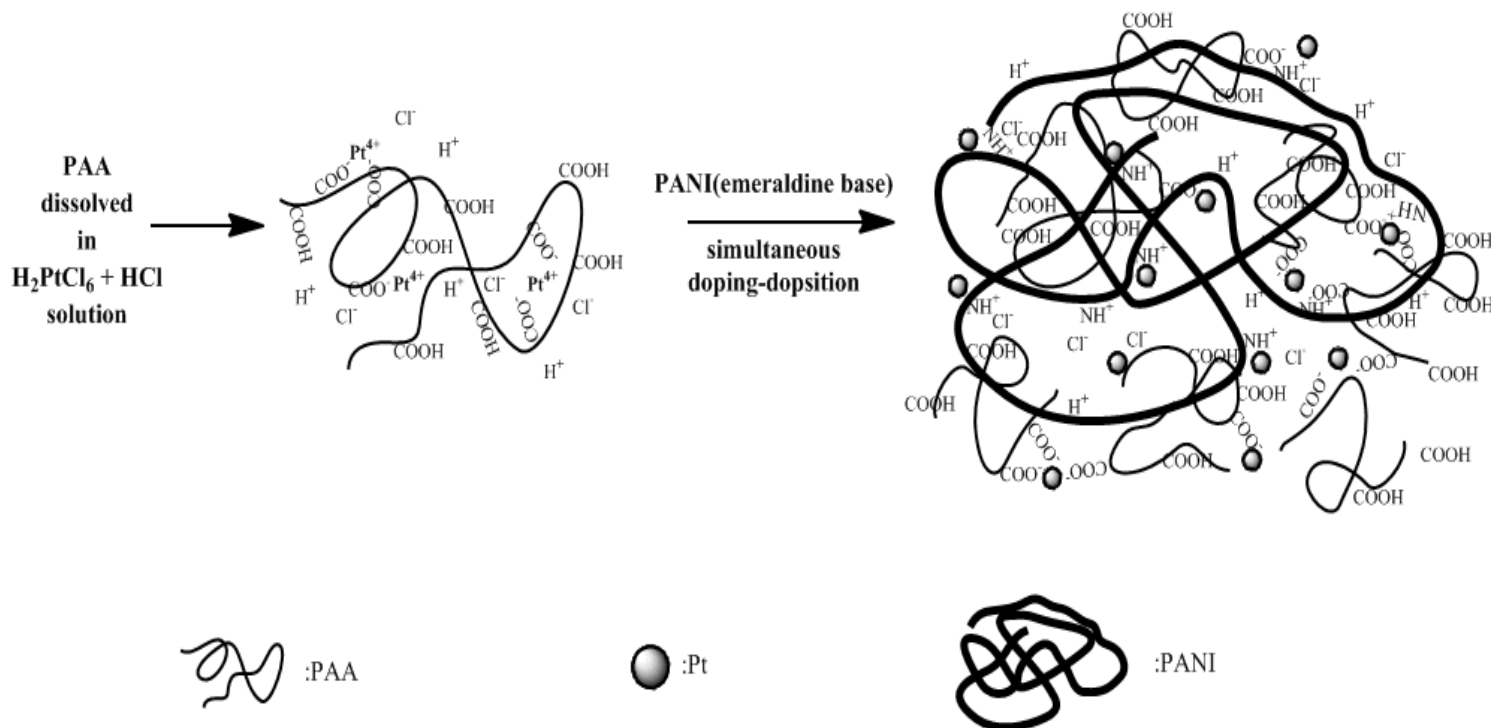


**Figure 5.** Schematic illustration for the formation of PANI-(PAA+HCl)-Pt.

#### 3.4. Electrocatalytic activity and stability of PANI-(PAA+HCl)-Pt for methanol oxidation

Cyclic voltammograms of PANI-HCl-Pt and PANI-(PAA+HCl)-Pt electrodes collected at a scan rate of  $10 \text{ mV sec}^{-1}$  in  $0.5 \text{ M H}_2\text{SO}_4$ , are shown in Fig. 6a-b, respectively. Three well-defined redox pairs can be seen due to the conversion of leucoemeraldine to emeraldine ( $0.2 \text{ V}$ , A/A' peaks), emeraldine to pernigraniline ( $0.7 \text{ V}$ , C/C' peaks), and hydroquinone to quinone ( $0.4 \text{ V}$ , B/B' peaks), respectively [27]. The PANI-HCl-Pt and PANI-(PAA+HCl)-Pt electrodes have a clear texture of hydrogen adsorption/desorption with no sharp peaks in the potential range of  $-0.2$  and  $+0.0 \text{ V}$  vs. Ag/AgCl [28]. There is a difference in the current density of hydrogen absorption and desorption between PANI-HCl-Pt and PANI-(PAA+HCl)-Pt electrodes. It is known that the integral of the intensity of hydrogen absorption and desorption represents the number of sites of Pt available for hydrogen adsorption and desorption, respectively [29,30]. The charge for hydrogen absorption and desorption on the PANI-(PAA+HCl)-Pt surface is  $5.44 \text{ mC cm}^{-2}$ , which is 2.0 times larger than that on the PANI-HCl-Pt surface ( $2.76 \text{ mC cm}^{-2}$ ). This implies that PANI-(PAA+HCl)-Pt has a higher surface area for Pt than that of PANI-HCl-Pt, which is attributable to the homogeneous dispersion of Pt in the PANI-(PAA+HCl) spatial network structure.

CV and chronoamperometry are convenient and useful tools for investigating the electrocatalytic activity and stability of electrodes for methanol oxidation, respectively. The methanol oxidation at PANI-HCl-Pt and PANI-(PAA+HCl)-Pt electrodes was characterized by CV in 0.5 M H<sub>2</sub>SO<sub>4</sub> solution containing 0.1 M methanol at a scan rate of 10 mV sec<sup>-1</sup>. The resulting cyclic voltammograms are shown in Fig. 7. Methanol oxidation commenced at about 0.4 V, with a peak at about 0.6 V. For the reverse scan, an oxidation peak occurred at about 0.55 V, and no reduction peak was observed. The onset potentials for methanol oxidation were 0.42 and 0.40 V for PANI-HCl-Pt and PANI-(PAA+HCl)-Pt, respectively. The lower onset potential of PANI-(PAA+HCl)-Pt is attributed to the -CO<sub>2</sub>H groups in PANI-(PAA+HCl) that can shuttle electrons easily (high positive charge nitrogen content) toward methanol oxidation.

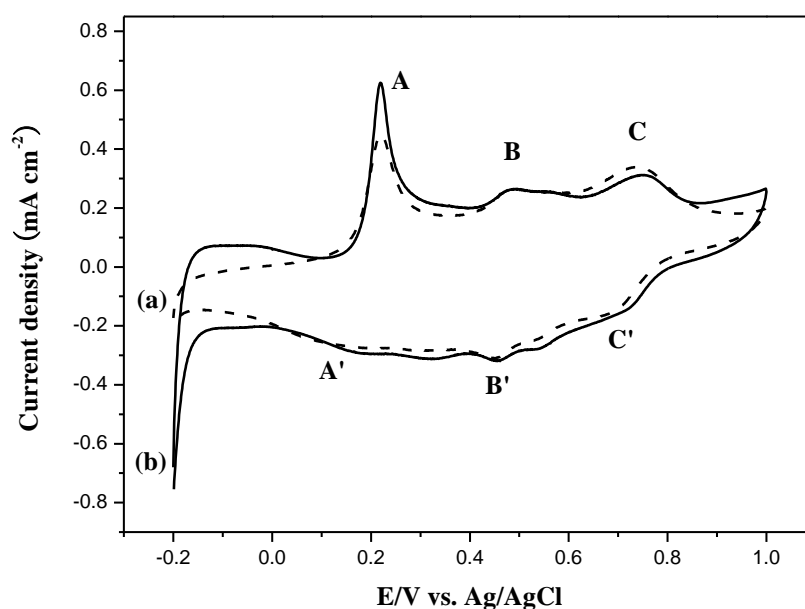


**Figure 6.** Cyclic voltammograms of (a) PANI-HCl-Pt and (b) PANI-(PAA+HCl)-Pt in 0.5 M H<sub>2</sub>SO<sub>4</sub> solution with a scanning rate of 10 mV sec<sup>-1</sup>.

A comparison of cyclic voltammograms for the oxidation of methanol on PANI-(PAA+HCl)-Pt and PANI-HCl-Pt electrodes indicates that the oxidation current at the PANI-(PAA+HCl)-Pt electrode is higher (curve b) than that at the PANI-HCl-Pt (curve a) electrode. For instance, the maximum anodic peak current density (*I*<sub>a</sub> in Table 2) of 25.1 mA cm<sup>-2</sup> mg<sup>-1</sup> observed for PANI-(PAA+HCl)-Pt electrode at about 0.60 V is higher than that for observed for PANI-HCl-Pt (12.1 mA cm<sup>-2</sup> mg<sup>-1</sup>). The better performance of the PANI-(PAA+HCl)-Pt electrode toward methanol oxidation may be attributed to the following reasons. Firstly, a high surface area for Pt particles is anticipated due to the uniform distribution of Pt particles into PANI doped with PAA and HCl, which can twist to form a spatial 3D matrix. Secondly, we anticipate that the -CO<sub>2</sub>H groups in PANI-(PAA+HCl) may act as a stabilizer for Pt particles and prevent the aggregation of Pt particles. The PANI-(PAA+HCl) matrix acts as a good medium for the deposition of Pt particles, and increases the density of active sites on the electrode surface.

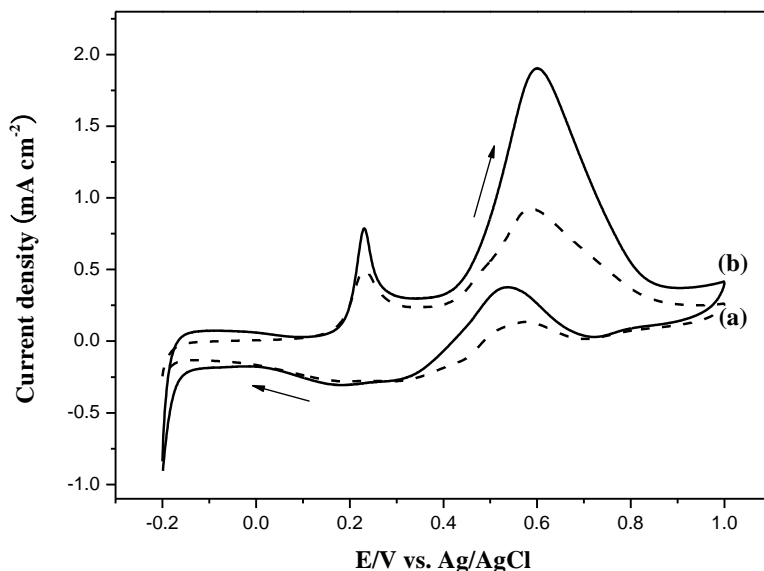


**Figure 7.** Cyclic voltammograms of (a) PANI-HCl-Pt and (b) PANI-(PAA+HCl)-Pt in 0.1 M CH<sub>3</sub>OH + 0.5 M H<sub>2</sub>SO<sub>4</sub> solution, scan rate = 10 mV sec<sup>-1</sup>.

**Table 2.** Components and characterizations for electrodes in the same deposition charge (0.1 C) of PANI as matrix.

Electrodes	Dopants	Charge of Pt deposition (C)	Concentration of methanol (M)	I <sub>a</sub> (mA cm <sup>-2</sup> ) / (mA cm <sup>-2</sup> mg <sup>-1</sup> )
PANI-HCl-Pt	HCl	0.150	0.1	0.9 / 12.1
PANI-(PAA+HCl)-Pt	PAA + HCl	0.150	0.1	1.9 / 25.1
PANI-PAMA-Pt <sup>a</sup>	PAMA	0.150	0.1	1.6 / 21.1
PANI-PSS-Pt <sup>b</sup>	PSS	0.144	1.0	1.5 / 21.0

<sup>a</sup>Reference [31].

<sup>b</sup>Reference [19].

The maximum anodic peak current density (I<sub>a</sub> in Table 2) of 25.1 mA cm<sup>-2</sup> mg<sup>-1</sup> observed for PANI-(PAA+HCl)-Pt electrode for the oxidation of methanol is higher than the 21.1 mA cm<sup>-2</sup> mg<sup>-1</sup> obtained for Pt in a polyaniline-poly(acrylic acid-co-maleic acid) (PANI-PAMA-Pt) electrode [31] for the same deposition charge of PANI and Pt. The higher current density for the PANI-(PAA+HCl)-Pt electrode may be due to the CO<sub>2</sub><sup>-</sup> groups of PAA helping the uptake of Pt<sup>4+</sup> ions by the PAA, HCl, and H<sub>2</sub>PtCl<sub>6</sub> solution. A uniform distribution of reduced Pt particles into PANI-(PAA+HCl) can twist to form a spatial 3D matrix. The oxidation current density (25.1 mA cm<sup>-2</sup> mg<sup>-1</sup>) for 0.1 M methanol oxidation observed for PANI-(PAA+HCl)-Pt is higher than that (21.0 mA cm<sup>-2</sup> mg<sup>-1</sup>) observed for PANI-PSS-Pt [19] for the oxidation of 1.0 M methanol (Table 2). Golabi and Nozad [32] reported that anodic current increases with increasing methanol concentration and levels off at concentrations higher

than 0.7 M. This might be attributed to the weak interaction between PANI and the  $-\text{CO}_2\text{H}$  groups of the weak acid PAA, which provides more network pore space with  $\text{Pt}^{4+}$  existence for facile preparing Pt nanoparticles. Hence, the proposed methods highly favor the formation of Pt nanoparticles in the PANI-(PAA+HCl) matrix via the “simultaneous doping-deposition” process.

Chronoamperometric responses at PANI-HCl-Pt and PANI-(PAA+HCl)-Pt electrodes for a solution of 0.1 M  $\text{CH}_3\text{OH}$  in 0.5 M  $\text{H}_2\text{SO}_4$  were recorded at 0.6 V (Fig. 8) and compared to evaluate the catalyst poisoning effect [33,34]. PANI-(PAA+HCl)-Pt has better catalytic properties toward methanol oxidation compared to those of PANI-HCl-Pt. For example, the current at 150 s is  $0.16 \text{ mA cm}^{-2} \text{ mg}^{-1}$  for PANI-(PAA+HCl)-Pt (curve b) and  $0.06 \text{ mA cm}^{-2} \text{ mg}^{-1}$  for PANI-HCl-Pt (curve a).

Furthermore, the methanol oxidation current decays at a lower rate for PANI-(PAA+HCl)-Pt than for PANI-HCl-Pt. This demonstrates that Pt particles embedded in PANI-(PAA+HCl) are more electroactive and stable compared to those in PANI-HCl. The incorporation of PAA into PANI may influence the formation of strongly absorbed poisonous species on the surface of Pt particles. Thus, the PANI-(PAA+HCl)-Pt electrode exhibited low catalyst poisoning.

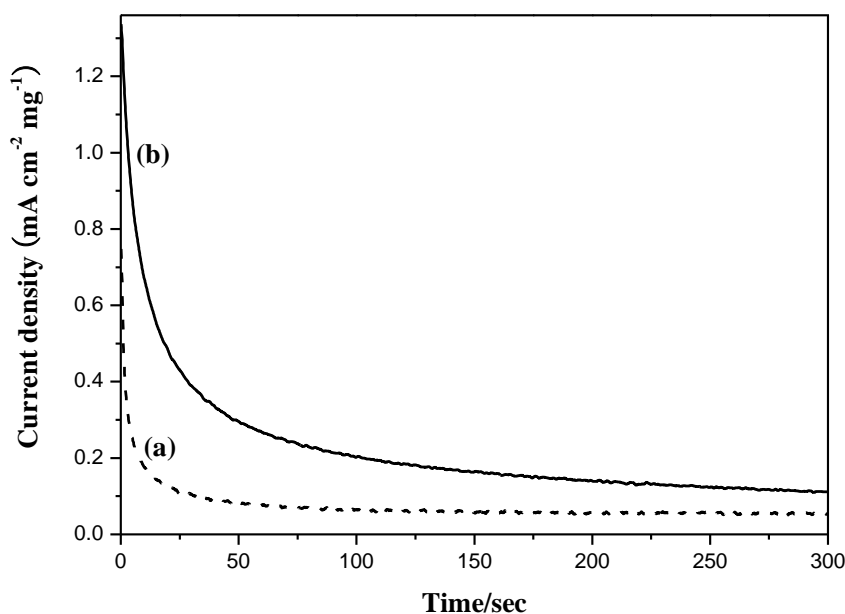


**Figure 8.** Chronoamperometric response of (a) PANI-HCl-Pt and (b) PANI-(PAA+HCl)-Pt at 0.6 V (vs. Ag/AgCl) in 0.1 M  $\text{CH}_3\text{OH}$  + 0.5 M  $\text{H}_2\text{SO}_4$  solution.

#### 4. CONCLUSIONS

PANI-(PAA+HCl) porous nanowires were synthesized by simultaneously doping PANI with PAA and HCl. The deposited Pt nanoparticles were incorporated into the PANI-(PAA+HCl) nanowire network structure to form the PANI-(PAA+HCl)-Pt composite electrode. The  $-\text{CO}_2\text{H}$  groups in the PANI-(PAA+HCl) spatial structure improve the stability of  $\text{Pt}^{4+}$  ions in the polymer matrix, resulting in a homogenous distribution of Pt in PANI-(PAA+HCl). The PANI-(PAA+HCl)-Pt electrode exhibits

a higher current density and lower onset potential toward methanol oxidation than PANI-HCl-Pt. The PANI-(PAA+HCl)-Pt composite electrode is a promising material for catalysts for methanol oxidation. The enhanced electrocatalytic activity of Pt in PANI-(PAA+HCl) opens up the possibility to using smaller amounts of Pt in DMFC applications.

#### ACKNOWLEDGEMENTS

The financial support of this work by the National Science Council of Taiwan under NSC 99-2218-E-151-003 is gratefully acknowledged.

#### References

1. B.D. McNicol, D.A.J. Rand, K.R. Williams, *J. Power Sources*, 83 (1999) 15.
2. M. Brandalise, M.M. Tusi, R.M.S. Rodrigues, E.V. Spinace, A.O. Neto, *Int. J. Electrochem. Sci.*, 5 (2010) 1879.
3. Y.I. Kim, D. Soundararajan, C.W. Park, S.H. Kim, J.H. Park, J.M. Ko, *Int. J. Electrochem. Sci.*, 4 (2009) 1548.
4. C.M. Bautista-Rodriguez, A. Rosas-Paletta, J.A. Rivera-Marquez, O. Solorza-Feria, *Int. J. Electrochem. Sci.*, 4 (2009) 60.
5. A.O. Neto, R.W.R. Verjullo-Silva, M. Linardi, E.V. Spinace, *Int. J. Electrochem. Sci.*, 4 (2009) 954.
6. J. Parrondo, R. Santhanam, F. Mijangos, B. Rambabu, *Int. J. Electrochem. Sci.*, 5 (2010) 1342.
7. B. Krishnamurthy, S. Deepalochani, *Int. J. Electrochem. Sci.*, 4 (2009) 386.
8. M. Brandalise, M.M. Tusi, R.M. Piasentin, M. Linardi, E.V. Spinace, A.O. Neto, *Int. J. Electrochem. Sci.*, 5 (2010) 39.
9. B. Pierozynski, D. Zielinska, *Int. J. Electrochem. Sci.*, 5 (2010) 1507.
10. M.S. El-Deab, *Int. J. Electrochem. Sci.*, 4 (2009) 1329.
11. B. Beden, F. Hahn, S. Juanto, C. Lamy, J.M. Leger, *J. Electroanal. Chem.*, 225 (1987) 215.
12. A.A. Hathoot, M. Abdel-Kader, M. Abdel-Azzem, *Int. J. Electrochem. Sci.*, 4 (2009) 208.
13. R.F.B. De Souza, M.M. Tusi, M. Brandalise, R.R. Dias, M. Linardi, E.V. Spinace, M.C. dos Santos, A.O. Neto, *Int. J. Electrochem. Sci.*, 5 (2010) 895.
14. J. Yano, H. Hirayama, Y. Harima, A. Kitani, *J. Electrochem. Soc.*, 157 (2010) B506.
15. F.J. Liu, L.M. Huang, T.C. Wen, A. Gopalan, *Synth. Met.*, 157 (2007) 651.
16. Y.C. Zhao, L. Zhan, J.N. Tian, S.L. Nie, Z. Ning, *Electrochim. Acta*, 56 (2011) 1967.
17. J. Li, X.Q. Lin, *J. Electrochem. Soc.*, 154 (2007) B1074.
18. V. Selvaraj, M. Alagar, I. Hamerton, *Appl. Catal., B Environ.*, 73 (2007) 172.
19. L.M. Huang, W.R. Tang, T.C. Wen, *J. Power Sources*, 164 (2007) 519.
20. C.W. Kuo, L.M. Huang, T.C. Wen, A. Gopalan, *J. Power Sources*, 160 (2006) 65.
21. F.J. Liu, *Polymer Composites*, 30 (2009) 1473.
22. T.C. Wen, L.M. Huang, A. Gopalan, *J. Electrochem. Soc.*, 148 (2001) D9.
23. Y.K. Zhou, B.L. He, W.J. Zhou, H.L. Li, *J. Electrochem. Soc.*, 151 (2004) A1052.
24. S.N. Kumar, G. Bouyssoux, F. Gaillard, *Surf. Interface Anal.*, 15 (1990) 531.
25. S.N. Kumar, F. Gaillard, G. Bouyssoux, A. Sartre, *Synth. Met.*, 36 (1990) 111.
26. L.D.D. Pra, S. Demoustier-Champagne, *Thin Solid Films*, 479 (2005) 321.
27. S.S. Chen, T.C. Wen, A. Gopalan, *Synth. Met.*, 132 (2003) 133.
28. C. Sivakumar, *Electrochim. Acta*, 52 (2007) 4182.
29. T.J. Schmidt, H.A. Gasteiger, G.D. Stab, P.M. Urban, D.M. Kolb, R.J. Behm, *J. Electrochem. Soc.*, 145 (1998) 2354.

30. A.Chen, D.J.L. Russa, B. Miller, *Langmuir*, 20 (2004) 9695.
31. C.C. Yang, T.Y. Wu, H.R. Chen, T.H. Hsieh, K.S. Ho, C.W. Kuo, *Int. J. Electrochem. Sci.*, 6 (2011) 1642.
32. S.M. Golabi, A. Nozad, *J. Electroanal. Chem.*, 521 (2002) 161.
33. X.J. Feng , Y.L. Shi, Z.A. Hu, *Int. J. Electrochem. Sci.*, 5 (2010) 489.
34. F.J. Liu, L.M. Huang, T.C. Wen, C.F. Li, S.L. Huang, A. Gopalan, *Synth. Met.*, 158 (2008) 603.